JOURNAL OF Materials CHEMISTRY

The effect of H^+ irradiation on the Cs-ion exchange capacity of zeolite-NaY

Binxi Gu,[a] Lumin Wang,[a] Shinxin Wang,[a] Donggao Zhao,[a] Victor H. Rotberg[b] and Rodney C. Ewing*[a]

[a]*Department of Nuclear Engineering and Radiological Sciences, University of Michigan, Ann Arbor, MI, 48109-2104, USA. E-mail: rodewing@umich.edu*
[b]*Ion Beam Laboratory, University of Michigan, Ann Arbor, MI, 48109-2104, USA*

Received 28th March 2000, Accepted 18th August 2000
First published as an Advance Article on the web 6th October 2000

Radiation effects on zeolite-NaY have been investigated by irradiation with a 500 keV H^+ beam. Zeolite-NaY suffers structural damage under proton irradiation. The crystalline-to-amorphous transition occurs at a total dose equivalent to an ionizing energy deposition of 3×10^{10} Gy and a displacement dose of 0.05 dpa (displacements per atom). The ion exchange capacity of the irradiated zeolite-NaY with 10 mM CsCl solution varies with the extent of damage to the crystalline structure. After 25 hours of exchange, the Cs-concentration in the amorphous region is $\sim$0.8 wt.%, which is much lower than in the undamaged region ($\sim$20 wt.%). This result confirms that radiation-induced amorphization can cause a significant loss of ion exchange capacity. The data also suggest that the radiation damage by proton radiation in zeolite-NaY is caused by both ionizing and displacement processes. Mechanisms related to the radiation-induced change in the ion exchange capacity are discussed.

1. Introduction

Zeolites have framework structures that contain channels and cavities. Cations and water molecules that are located in the cavities give rise to a high ion-exchange capacity that leads to a variety of applications for zeolites in nuclear waste treatment processes. Zeolites are used for the selective removal of radionuclides, such as caesium, strontium, rare-earths, and actinides, from the high-level liquid nuclear waste generated from nuclear fuel reprocessing, as well as the decontamination and decommissioning of nuclear facilities.[1–3] Zeolites are also considered as a potential back-fill material in nuclear waste repositories[4] and as suitable waste forms after thermal/hydrothermal treatment.[5,6] Once radionuclides are incorporated into zeolites, they will be subjected to high radiation doses due to radioactive decay. For commercial high-level nuclear waste forms with a 25 wt.% waste loading, the cumulative ionization dose from β-decay events can be as high as 10^{10} Gy after 100 years, and the anticipated dose from α-decay may reach 7×10^8 Gy in 1000 years.[7] The structures and properties of zeolites in a radiation field will thus determine the extent of containment of the radionuclides. Zeolite-group phases have also been identified as precipitates on the corroded surfaces of nuclear waste glasses.[8] The properties of these surface layers significantly affects radionuclide release from nuclear waste forms. Rare-earths, actinides, Cs, and Sr are retained in these alteration products through ion exchange reactions.[8,9]

Previous studies have shown that zeolites are susceptible to both radiation- and thermally-induced amorphization.[10,11] Complete amorphization can be induced by an ionization process with 10^{10}–10^{11} Gy of ionizing energy deposition under electron irradiation or by direct displacement damage processes at a cumulative dose as low as 0.1 dpa under ion beam irradiation.[10] Analcime and zeolite-5A were found to lose their long-range order at doses of 0.1 dpa and $\sim 6 \times 10^8$ Gy with $1 \sim 1.5$ MeV krypton irradiation.[12,13] Structural damage in zeolite-A has been noted under neutron irradiation. Complete collapse of the crystalline structure occurred at a dose of 7×10^{23} n m^{-2}.[14] Thermally-induced amorphization of zeolite-NaY can cause a significant change in the ion exchange and retention behavior for radionuclides, such as Cs and Sr.[11]

Most of the previous research on the ion exchange capacity of zeolites has concentrated on the effects of time, solution temperature, chemistry and pH.[15–20] Little effort has been made to evaluate the effects of radiation-induced structural changes on the adsorption and desorption properties of zeolites. Palau and Pillay[21] reported that the Cs-exchange capacity of IE-95 zeolite decreased by $\sim$3% at a cumulative dose of 50 MGy, which contradicts other results measured from the same material.[22] High dose (100 MGy) gamma irradiation of IE-95 zeolite was found to have little effect on the crystalline structure and ion exchange capacity. Daniels and Puri[23] have shown that gamma irradiation of zeolite-4A resulted in a reduced ion exchange capacity for Cs, and this was attributed to the displacement of Na into sodalite cages *i.e.* the "lock in" sites. Although a similar displacement mechanism was proposed for the neutron irradiation of zeolite-4A and gamma irradiation of zeolite-13X, no appreciable change in the exchange capacity was observed after irradiation.[24,25] The discrepancies among these results are attributed to the inherent difficulties in measuring dose and radiation effects at high doses. In order to achieve an amorphization dose of 10^{10}–10^{11} Gy, as determined by electron beam irradiation, 50 years of irradiation are required for available γ-sources. Although heavy ion and electron irradiations can reach high radiation doses and produce appreciable damage to the crystalline structure in a short period of time, the volume of the damaged region is usually too small to perform chemical measurements, such as ion exchange and leaching experiments.

In the present study, zeolite-NaY was irradiated with energetic protons at a flux of 5×10^{12} ions s^{-1} cm^{-2} so that significant damage was produced in a volume large enough for chemical experiments. Instead of analyzing the solution chemistry to determine the changes of chemical properties of the irradiated material, electron microprobe analysis (EMPA), transmission electron microscopy (TEM) and scanning electron microscopy (SEM) were used to study the change in ion exchange capacity as a function of the extent of damage to the crystalline structure.

 DOI: 10.1039/b002473m

2. Experimental

2.1 Materials

Zeolite-NaY (Si/Al = 2.55), which contains 13.0 wt.% Na_2O, was obtained from the Zeolyst International Company in powder form. The ideal chemical composition of the zeolite-NaY is $NaAlSi_2O_6 \cdot nH_2O$. Zeolite-Y is structurally similar to faujasite, which has an aluminosilicate framework structure with large channels and cages inside the structure. As illustrated in Fig. 1, there are three different types of cages in the faujasite-type structure: supercages, sodalite cages (the β-cage), and double 6-ring prisms. Each supercage is connected to four other supercages *via* a 12-ring "window" with a free aperture of 0.77 nm. The sodalite cages, which are connected to four adjoining supercages *via* 6-ring openings of 0.22 nm, are linked together by the double 6-ring prisms. Exchangeable cations are located in all three types of cages. The distribution of cations depends not only on the properties of each cation, but also on the level of dehydration. The size of the free aperture plays an important role in determining the features of the ion exchange reaction for particular cations. Approximately two-thirds of the exchangeable cation sites are located in supercages.

2.2 Experimental procedures

2.2.1 H^+ Beam irradiation. Zeolite-NaY powders were pressed to form tablets at room temperature to a pressure of ~17 MPa. The tablets were 2 cm in diameter and 1.5 mm thick. The pressed samples were analyzed by X-ray diffraction and no structural change was detected. The density of the tablet was 0.8 g cm^{-2}, as determined by geometric measurements. The zeolite tablets were irradiated with a 500 keV H^+ beam generated by a tandem ion beam accelerator at the Michigan Ion Beam Laboratory. The samples were irradiated with a scanned beam over an area of 2.5×2.5 cm^2 for 10, 20 and 30 hours with the current density maintained at ~0.8 μA cm^{-2}. The corresponding dose rate was $\sim 5 \times 10^{12}$ ions s^{-1} cm^{-2}. The cumulative doses were also measured with a Faraday cap, which yielded total doses of 2×10^{17}, 4×10^{17}, and 6×10^{17} ions cm^{-2} for the three samples, respectively.

2.2.2 Structure determination by TEM. Changes in the microstructure of the irradiated zeolite-NaY were observed using TEM. High resolution TEM was performed using a JEM 4000EX electron microscope operated at 400 kV. The cross-sectional TEM sample was prepared by sealing the sample in M-bond 610 provided by M-line Accessories, Measurement Group, Inc. The sample was mechanically polished followed by small angle 3–5 keV Ar ion milling. No observable damage was produced from sample preparation, as determined by high resolution TEM.

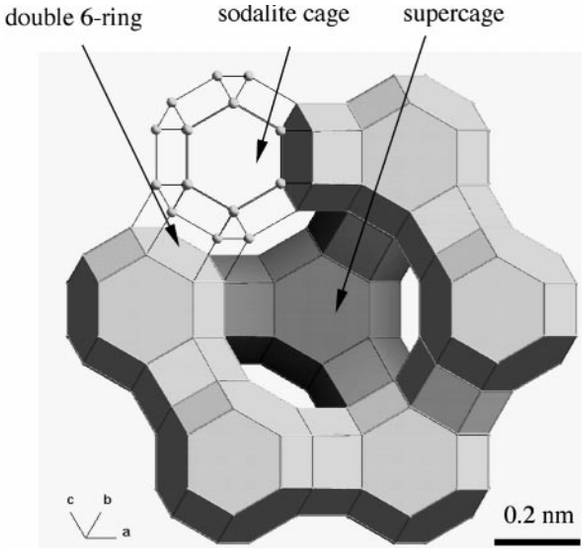

Fig. 1 Schematic diagram of the zeolite-Y structure.[31]

2.2.3 Ion exchange. The irradiated zeolite samples were placed in a 10 mM CsCl solution at room temperature for 25 hours without agitation. The solid : solution ratio was 50 mg zeolite : 50 mL solution. Because the density of the pressed sample was only ~50% of the theoretical density, the samples contained a large amount of void space. The large inter-particle pore size allowed the CsCl solution to quickly diffuse into the interior of the samples and ensured that all the particles were in effective contact with the solution throughout the ion exchange experiment. Based on a previous study,[11] a complete Cs-zeolite-NaY ion exchange reaction occurred almost instantly under stirred conditions. We have therefore assumed that the entire sample reacted with the Cs-solution thoroughly and reached equilibrium after 25 hours of immersion. No significant dissolution was observed during the ion-exchange experiment. The samples were rinsed with deionized water at the end of the ion exchange reaction and dried in air at 45 °C for 48 hours.

2.2.4 Chemical composition determination by SEM and EMPA. The irradiated zeolite-NaY samples, loaded with Cs, were mounted in epoxy resin and polished for SEM and electron microprobe analysis. The sample surface was coated with a carbon film to avoid charge accumulation. SEM was performed using a Philips XL30 field emission gun scanning electron microscope operated at 10 kV. Samples were examined under both SE (secondary electron) and BSE (backscattered electron) modes. Chemical analysis with SEM was conducted through energy dispersive X-ray spectroscopy (EDS). The elemental distributions on the cross-sections of the irradiated samples were measured for Cs and Na, respectively, with the dwelling time set at 100 μs. Approximately 10,000 frames were recorded for each test. The cross-sectional samples were also analyzed with a Cameca CAMEBAX electron microprobe analyzer employing wavelength dispersive system (WDS) to further quantify the change in ion exchange capacity as a result of irradiation. The Cameca PAP correction routine $\phi(\rho z)$, *i.e.*, modified ZAF by Pichou and Pichouir,[26] was used for data reduction. The chemical composition of Cs-exchanged zeolite-NaY was analyzed using a focused beam in point mode and a raster beam with a beam size of 1.5×1.5 μm. The electron microprobe was operated at an accelerating voltage of 15 kV with a current of 10 nA. Six compound standards with their detailed compositions listed in Table 1 were used for calibrating the concentrations of the six elements measured in the samples.

3 Results and discussion

3.1 Structure

Monte Carlo simulation with the SRIM 2000 code[27] was used to estimate the depth distribution of energy loss and displacement production for proton irradiation of zeolite-

Table 1 Standards used for EMPA

Element	Standard: formula/name
Na	$NaAlSi_3O_8$/Albite
Mg	$MgSiO_3$/Synthetic enstatite
Al	Al_2SiO_5/Andalusite
Si	$KAlSi_3O_8$/K-feldspar
Ca	$CaSiO_3$/Wollastonite
Cs	$(Cs,Na)_2Al_2Si_4O_{12} \cdot H_2O$/Pollucite

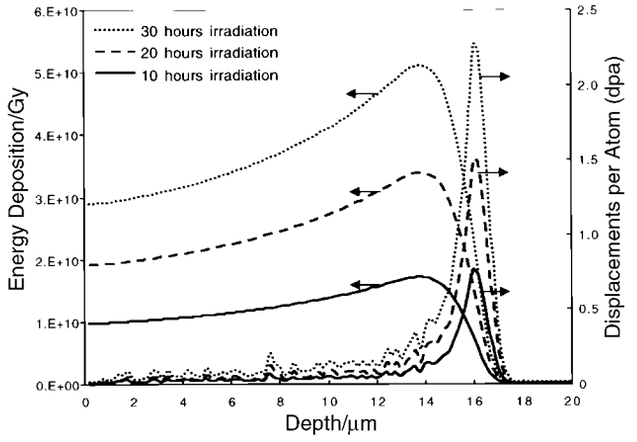

Fig. 2 The energy deposition and displacement production profiles along the depth of proton penetration for samples with irradiation doses of 2×10^{17} ions cm^{-2} (10 hours), 4×10^{17} ions cm^{-2} (20 hours), 6×10^{17} ions cm^{-2} (30 hours), respectively.

NaY. In order to predict the dose effect on the damage process, the energy loss of individual protons was converted to ionizing energy deposition (Gy). Fig. 2 shows the variation of ionizing energy deposition as a function of the depth from the irradiated sample surface for the samples irradiated for 10, 20 and 30 hours, respectively. The energy deposition increases with the increase in depth and reached a maximum at 13.5 μm from the surface for all three samples. Based on the assumption of a displacement energy of 25 eV for all elements in the target, the total number of displacements per atom (dpa) in the target was calculated for the different cumulative doses and are shown in Fig. 2. Unlike the energy deposition, the majority of collision events occurred within a narrow band 16 μm from the surface. For samples with a density of 0.8 g cm^{-2}, the SRIM 2000 simulation predicts that the average longitudinal ion range is 16.1 μm with a range straggle of 0.7 μm. These results indicate that the damage peak resulting from the nuclear collisions was located at a depth of ~16 μm where most of the protons are fully stopped. The structural and morphological changes of zeolite-NaY after irradiation were determined by high resolution TEM and selected area electron diffraction (SAD). Fig. 3 shows the bright field micrograph of the cross-section of zeolite-NaY irradiated for 20 hours. The boundary between the

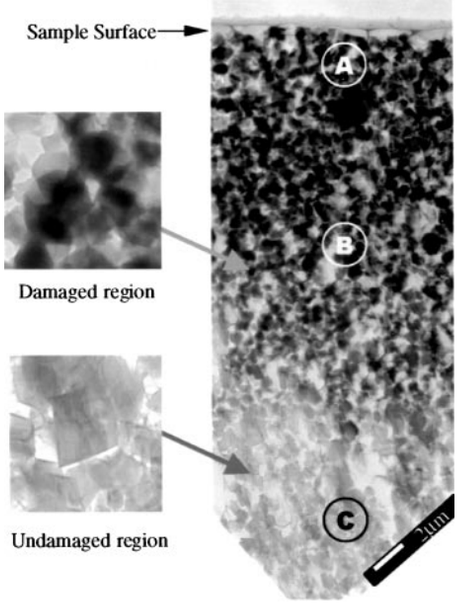

Fig. 3 TEM bright field image of the cross-section of irradiated zeolite-NaY.

irradiated and unirradiated regions is evident from the different contrast between the two regions. The increase of dark contrast in the irradiated region is attributed to an increase in the atomic density. The increase of the atomic density in the neutron-irradiated zeolite has also been observed by Rees and Williams[14] using X-ray and density measurements. The enlarged TEM images in Fig. 3 reveal that the structural damage was accompanied by a change in particle morphology. The sharp edges of the particles before irradiation have become rounded as a result of irradiation. A similar phenomenon has also been observed for zeolite-L[28] and zeolite-A.[29] The change in the particle density and appearance is an indication of the collapse of the framework structure due to irradiation. Because zeolite-NaY consists of large channels and voids, the material densifies when the framework collapses. Fig. 4 shows high-resolution lattice images and SAD patterns taken from different locations as labelled in Fig. 3. In the region directly below the irradiated sample surface, the crystalline structure of zeolite was partially damaged, as indicated by the loss of lattice contrast and the lower intensity of the Bragg diffraction maxima, as shown in Fig. 4(A). Based on the SRIM calculation, the energy deposition of 500 keV proton ions is 1.9×10^{10} Gy at the sample surface, while elastic collisions of protons with target nuclei produce ~0.01 dpa damage. In the peak damage region where the energy loss of incident particles and collisional displacement damage have reached a maximum, the atomic-scale periodicity of the crystal was completely destroyed. The amorphization of the material is evident by the complete loss of lattice contrast in the high resolution TEM image, the disappearance of diffraction maxima, and the presence of amorphous diffraction haloes (Fig. 4(B)). The energy deposition in the amorphized zeolite is $\sim 3 \times 10^{10}$ Gy, which is an order of magnitude lower than the dose required for electron radiation-induced amorphization at room temperature.[10] This result suggests that the temperature rise due to beam heating may contribute to the damage of the crystalline structure. Because the target material was porous and had a very low thermal conductivity, beam heating was not negligible. The zeolite tablets were clamped to a metal stage in a vacuum, and there was effectively no heat transfer by conduction. The temperature rise in the sample was therefore calculated by assuming that all the heat was dissipated by radiation from the front and back surfaces of the sample. When the ion beam scanned the entire target surface, the equilibrium temperature rise in the target material could be calculated from the following equation:[30]

$$IE = 2\varepsilon\sigma(T_T^4 - T_0^4) \quad (1)$$

where I is the ion beam current in amperes, E is the ion energy in electron volts, ε is the thermal emissivity of the surface, σ is the Stefan–Boltzmann constant (5.67×10^{-12} W cm^{-2} K^{-4}), T_T is the temperature of the target in K, and T_0 is the temperature of the surroundings in K.

The target temperature calculated from the above equation was 266 °C, which was well below the thermal amorphization temperature of 760–800 °C for zeolite-NaY.[31] However, this

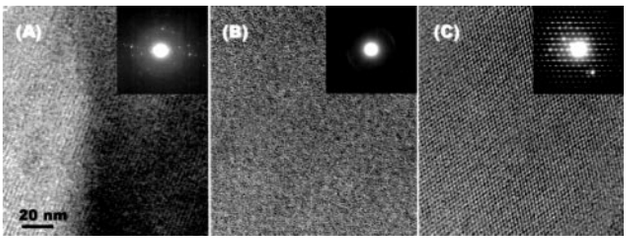

Fig. 4 High resolution TEM lattice images and SAD patterns from the locations labelled in Fig. 3: (A) near the surface, (B) fully-damaged region, and (C) undamaged region.

temperature is high enough to cause a dramatic decrease in the amorphization dose of zeolite-NaY. Based on the electron beam irradiation data,[10] the amorphization dose at 300 °C drops to ~30% of the value obtained at room temperature. Electron diffraction patterns of the cross-sectioned TEM sample confirmed that no structural damage was produced in the region adjacent to the radiation damaged area, where temperature may have reached ~260 °C (Fig. 4(C)).

3.2 Ion exchange capacity

The irradiated zeolite-NaY samples were loaded with Cs by an ion exchange reaction. When zeolite-NaY was placed in contact with the CsCl solution, exchangeable sodium ions in the supercages of the zeolite were extracted into the solution and the cation sites in the zeolite were then occupied by caesium ions from the solution. For zeolite-NaY the ion exchange capacity is determined by the nature of the cation species, size, and charge. Because the Cs ion is larger than the 6-ring aperture in the sodalite cages and double 6-ring prisms, the Na–Cs exchange reaction can only occur in the supercages. Approximately 30% of the Na ions are located in the small cages, and these cations cannot be exchanged by Cs under normal conditions. Fig. 5 shows the elemental distribution of Cs and Na, as determined by EDS mapping on the cross-section of irradiated zeolite-NaCsY. Signals from K-line and L-line X-rays were recorded for Na and Cs, respectively. The bright contrast on the elemental maps represents a higher elemental concentration. The different contrast between the radiation-damaged and undamaged regions is clear in the Na distribution map. The contrast difference can be more clearly seen from the intensity profile produced from the elemental mapping. In the radiation-damaged region, the Na-concentration is higher than in the undamaged region, indicating that less Na was exchanged by Cs after the structure was damaged. Although the contrast difference for Cs was not as obvious as for Na due to the low X-ray counting rate from the L-line X-rays of Cs, a darker band can still be seen in the damaged region of the Cs map. This result further confirmed the decrease in the ion exchange capacity upon radiation-induced structural damage. Fig. 6 is an SEM BSE image of the cross-section of the Cs-exchanged zeolite-NaY sample after irradiation with a 500 keV proton beam to 4×10^{17} ions cm^{-2}. The contrast in the BSE image is atomic number dependent, *i.e.* the material containing heavier elements gives rise to brighter contrast. The

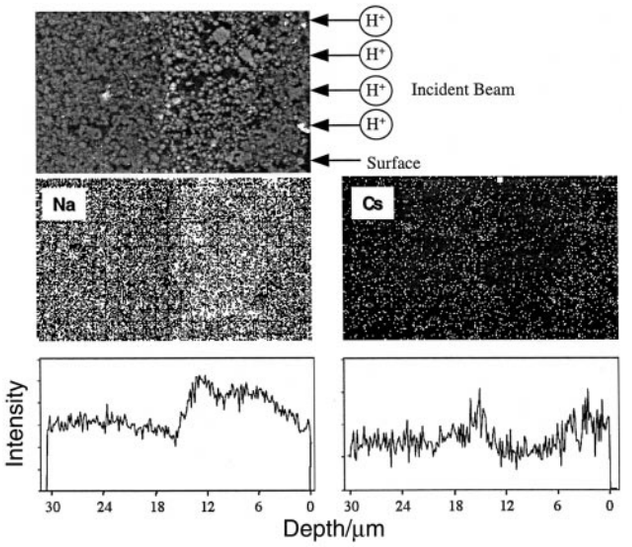

Fig. 5 Elemental distribution of Na and Cs on the cross-section of irradiated zeolite-NaY exchanged with Cs. The intensity profiles at the bottom of the diagram were obtained based on the contrast in the elemental maps.

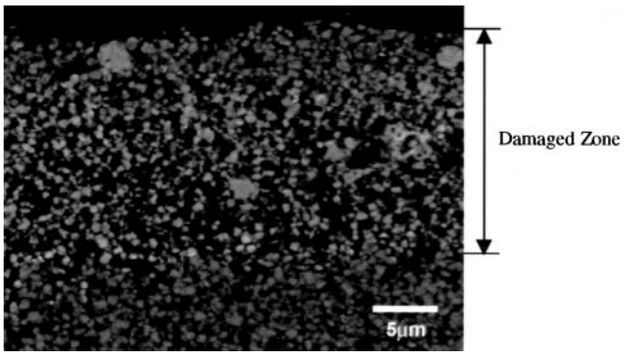

Fig. 6 SEM BSE image of proton irradiated zeolite-NaY loaded with Cs. The sample was irradiated by H^+ to a total fluence of 4×10^{17} ions cm^{-2}. The width of the damaged band is approximately 17.5 μm.

beam-damaged region can easily be differentiated from the undamaged region by the difference in the particle morphology. The width (~17.5 μm.) of the radiation-damaged region can be measured directly from Fig. 6. Fig. 6 also shows a similar morphological change (*i.e.* the shrinkage of the particles), as was observed by TEM. In the undamaged area, there are isolated aggregates in the zeolite matrix with higher contrast. This may be attributed to the higher concentration of heavy elements, such as Cs, which exist as a secondary phase in ion-exchanged zeolite. The existence of a Cs-rich phase in the Cs-exchanged zeolite-NaY has been observed in a previous X-ray diffraction study[11] and was further confirmed by electron microprobe analysis in this work.

To further quantify the radiation effects on the ion exchange capacity of zeolite-NaY, we performed detailed measurement of the concentrations of Cs and other elements along the cross-section of the irradiated samples. Most of the experiments were conducted in the raster beam mode, in which the beam scanned over an area of 1.5×1.5 μm. This beam size is larger than the average particle size of the sample. The information gathered from each point is therefore an average concentration from an aggregate of several zeolite particles. Fig. 7 shows the variation of Cs-concentration as a function of depth from the irradiated sample surface. For the sample irradiated for 20 hours, the Cs-concentration decreased gradually with increasing target depth and reached the lowest concentration (~1 wt.%) at 12 μm, indicating that the ion exchange capacity decreased with increasing radiation damage. When the zeolite was irradiated for a longer time, *i.e.* up to 30 hours, the region with the lowest Cs-concentration widened. However, the Cs-concentration did not decrease further with an increase of ionizing energy deposition, this suggests that once complete amorphization is reached, further radiation does not have an effect on the ion

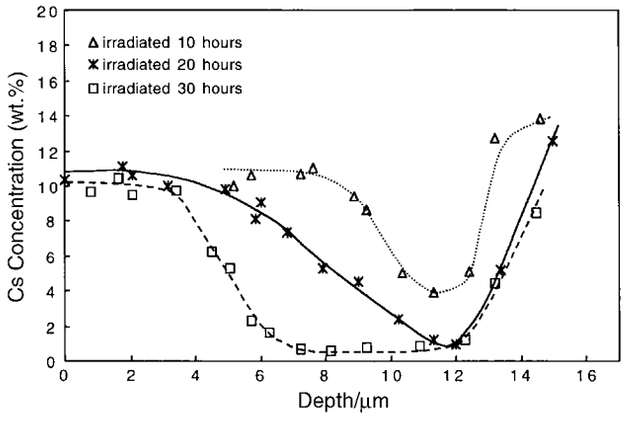

Fig. 7 The variation of Cs-concentration, as a function of target depth for the samples irradiated with 500 keV H^+ for 10, 20 and 30 hours.

exchange capacity. From Fig. 7 and Fig. 2, we may determine the amorphization dose, $\sim 3 \times 10^{10}$ Gy, by assuming that the point of lowest dose, at which the lowest Cs-concentration occurs, is the amorphization dose. This assumption is supported by high resolution TEM and SAD, *i.e.* in the region corresponding to the lowest Cs-concentration the crystalline structure is fully damaged. The concentration profiles in Fig. 7 and the energy deposition profiles in Fig. 2 suggest that the radiation damage to the zeolite by energetic protons is dominated by an ionization mechanism in the low displacement rate region. According to Fig. 2, the damage produced by nuclear collision processes should be restricted to a narrow band with an abrupt structural and Cs-concentration change in the region at the end of the ion range. However, the wide range of low Cs-concentration in the sample irradiated for 30 hours and the gradual decrease in Cs-concentration with increasing target depth in the 20 hour irradiated sample indicates that the extent of structural damage and the change in ion exchange capacity are a function of the ionizing radiation dose. For the sample irradiated for 10 hours, even at the peak damage region, the Cs-concentration did not reach a Cs-concentration as low as in the cases of higher dose irradiations. This result supports the suggestion that ionizing radiation is the dominant process leading to structural damage. The average Cs-concentration measured in the undamaged region was ~ 20 wt.%. A measurement of Cs-concentration in the point mode by EMPA showed that the average Cs-concentration in the bright spots is 30–50% higher than in the undamaged zeolite matrix. Fig. 8 shows the change of concentration for all cations in the zeolite-NaCsY sample irradiated for 30 hours. Although the measured Na-concentration is lower than the actual concentration due to the migration of Na under the electron beam during the electron microprobe analysis, Fig. 8 shows that the Na-concentration profile moves in the opposite direction as compared with the Cs-concentration. No significant concentration changes were observed for Al and Si.

3.3 Radiation damage and ion exchange capacity

Two processes occur when protons travel through the zeolite target. The protons lose energy primarily by ionization. Once the proton slows sufficiently, nuclear collisions between protons and target nuclei become the dominant mechanism of energy loss. Based on the SRIM 2000 simulation, 99.75% of the energy loss by a proton is by ionization, indicating that ionizing irradiation plays an important role in damaging the zeolite-NaY structure. Also based on the SRIM 2000 calculation, the damage due to the displacement events should occur primarily in a narrow band at the end of the ion range. The number of displacement events in the peak damage region (*e.g.* ~ 1.5 dpa for the sample irradiated for 20 hours) is two orders of magnitude higher than on the surface

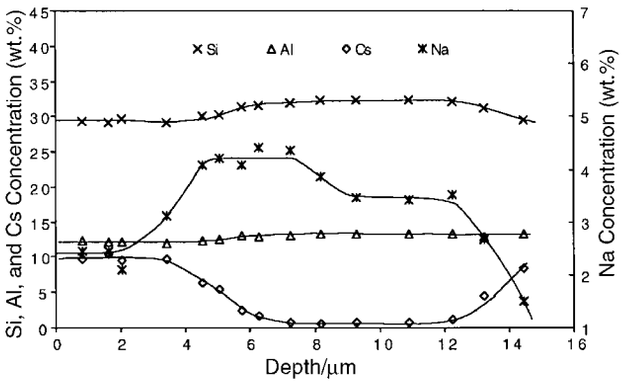

Fig. 8 Concentration profiles of major elements in the irradiated zeolite-NaCsY. The sample was irradiated with a 500 keV proton beam for 30 hours.

(~ 0.01 dpa). On the other hand, the ionizing energy loss of a proton along its path increases gradually, with the point of maximum energy loss located at a distance slightly less than the ion range (16.1 μm). The experimentally observed structural and ion exchange capacity changes as a function of proton penetration depth are consistent with the role of the ionization process, as the structural damage accumulates gradually in contrast to an abrupt change that would be expected from the displacement production profile. However, the displacement damage cannot be ignored, because the displacement of atoms in the target may play an important role in the decrease in the ion exchange capacity. The displacement doses in the peak damage region (0.8, 1.5, 2.3 dpa for the proton fluences of 2×10^{17} ions cm^{-2}, 4×10^{17} ions cm^{-2}, 6×10^{17} ions cm^{-2}, respectively) are significant as compared with the amorphization dose of 0.1 dpa obtained from the Kr^+ irradiation of zeolite-NaY.[10] Even on the sample surface, the total damage is on the order of 0.01 dpa.

There have been several mechanisms proposed for the radiation-induced crystalline-to-amorphous transition,[10,28] yet none have been applied to explain the effect on the ion exchange capacity of zeolites. Most of the mechanisms proposed for ionizing radiation-induced damage are associated with the breaking of Al–O bonds in the zeolite framework. The importance of the decomposition of zeolitic water by a radiolysis reaction has long been recognized.[32] For hydrated zeolite, large numbers of hydroxyl ions may be produced along the path of protons. At least two damage processes may occur.[28] In one process, the OH^- radicals may strip away the non-framework cations and leave catalyically active centers near the aluminium sites. At these centers, the Al–O bond may be weakened because of charge imbalance or even broken to form peroxy linkages. Another mechanism involves the interaction of H^+ produced by the radiolysis of water with the oxygen in Al–O–Si bridges. The proton may preferentially weaken the Al–O bond and convert the framework Al into a non-framework Al. The preferential breaking of the Al–O bond in the Al–O–Si bridges has been observed in the hydrothermal stabilization of zeolites.[33] Both mechanisms suggest that the removal of water from the supercage increases the stability to ionizing radiation.[33,34] The fundamental unit of the zeolite-NaY structure is the SiO_4 tetrahedral monomer. The substitution of Al for Si in the framework structure causes a charge deficiency near the Al sites, which is balanced by introducing additional cations such as Na, into the specific sites in the zeolite cages. Once one of the Al–O bonds in the tetrahedron is broken, Al can still be coordinated to three oxygens, and the structure remains stable.[33] The pendant oxygen tends to attract the highly mobile non-framework cations and form a strong Na–O bond. In this case, less exchangeable cations will be available for ion exchange. In our experiment, significant dehydration may occur during the irradiation, as the sample temperature may reach 250 °C due to beam heating. As demonstrated by Norby *et al.*[35] with Cs-exchanged zeolite-NaY, approximately 90% of the water is lost between 50–200 °C, but complete dehydration occurs when the temperature reaches 450 °C. Other researchers have shown that complete dehydration usually occurs at temperatures above 350 °C.[31] However, structural damage due to radiolysis may still be significant even with only trace amounts of water remaining in the structure. A thermal study of the collapse of the zeolite structure by the dealumination mechanism has indicated that trace amounts of water are sufficient to interact with the Si–O–Al bond and cause Al–O bond breakage.[36] Even in the absence of water, the crystalline-to-amorphization transition can still occur in zeolites, as observed in fully dehydrated zeolite-Y and zeolite-A.[37,38]

Other mechanisms, which differ from those mentioned above for hydrated zeolite, may be involved in the damage process. Because the zeolite structure contains a large proportion of

void space and is maintained by a delicate charge balance, the structure is relatively unstable. Even small changes to the atomic arrangement inside the framework and cages may lead to the collapse of a large number of atoms in the surrounding area. Direct observation of the amorphization of zeolite using high resolution TEM[32] suggests that ionizing radiation can preferentially breakdown the relatively weakly bonded structural units. The displacement of Na^+ by direct collision and ionization processes may thus play an important role in the destruction of the structure and the loss of ion exchange capacity. This is particularly true in the case of proton irradiation of zeolites. The probability of Na being displaced is high as compared with other framework cations in the structure, because Na is loosely bonded and becomes highly mobile under the impact of the electromagnetic field exerted by the moving protons. The Na-concentration in the probed area was found to be significantly lower than the bulk concentration of zeolite-NaY when the electron microprobe was operated in point mode. A more detailed study of K-exchanged zeolite-L[28] showed that up to 60% of the exchangeable cations may be displaced, with about 20% lost from the crystal when the zeolite is exposed to a focused electron beam. Two possible mechanisms have been proposed for the observed variation of cation concentration under electron beam irradiation:[39] (i) preferential sputtering of the alkali elements; (ii) diffusion of the alkali elements within the specimen. The displacement of Na may affect the ion exchange capacity in two ways:

(1) By causing the breakdown of weakly bonded Al–O as the charge-balancing cation is removed. As explained previously, the breakdown of the Al–O bond may lead to stronger bonding between oxygen and Na^+ and consequently reduce the availability of exchangeable cations.

(2) Reducing the number of exchangeable cations by moving them from exchangeable sites to non-exchangeable sites. Lai and Rees[40,41] have demonstrated, using the Szilard–Chalmers cation recoil technique, that cations may be displaced from supercages to "lock-in" sites or *vice versa* by neutron irradiation. Daniels and Puri[23] have attributed the reduction of the Cs-exchange capacity of zeolite-4A under gamma irradiation to the displacement of exchangeable cations into locked-in sites.

The simplest explanation for the dramatic loss of ion exchange capacity in the amorphous zeolite is the collapse of the framework structure. As observed in the present study and by a number of other researchers,[28,42] the amorphization of zeolite is usually accompanied by distortion and shrinkage of the crystal. This is an indication that in the amorphized zeolite atoms are closer to one another and the large voids have become smaller or even disappeared. The relative sizes of the ions in solution and the apertures in the crystalline structure determine whether or not the ion exchange reaction can proceed. For Cs-ion exchange, the reaction can only occur in the supercage for which the aperture size is larger than the Cs ion. When the crystalline structure collapses, the aperture shrinks, and exchangeable cations are trapped inside the structure. As suggested by Acosta *et al.*,[29] the amorphization of zeolite-CaA under electron beam irradiation is initiated from localized sites, such as the apertures of the channels, *i.e.* the apertures of the channels are more susceptible to radiation damage. This suggestion has been supported by the changes in the dimensions of the channels observed in the high resolution TEM image.[29]

We emphasize the similarities between radiation- and thermally-induced amorphization, in particular their effects on the ion exchange capacity of zeolites. A previous study[11] has shown that similar morphological changes occurred when the crystalline-to-amorphous transition of zeolite-NaY occurred at 900 °C. The thermally-induced amorphization can cause up to 95% loss of the ion exchange capacity for Cs, which is consistent with the result obtained in the proton irradiation study. These results imply that collapse of the zeolite-NaY structure, either by radiation or thermal treatment, may have some effect on the ion exchange capacity. Indeed, there have been a number of studies showing that the collapse of the zeolite structure by thermal treatment also begins with breakage of the Al–O bond.[31,36] The similar properties of radiation- and thermally-induced amorphous phases suggest that thermal treatment, which can be performed much more easily and economically than the irradiation of bulk material, may be a useful method for simulating the radiation effects on materials with microporous structures, such as zeolites.

4. Conclusions

The amorphization of zeolite-NaY has been induced by a 500 keV proton irradiation. The ionizing dose required to achieve amorphization under proton irradiation is $\sim 3 \times 10^{10}$ Gy which is approximately an order of magnitude lower than the electron beam irradiation-induced amorphization dose.[10] The temperature rise due to beam heating is probably the cause of the lower ionizing amorphization dose. Both ionizing and elastic interactions of the proton bombardment are responsible for the collapse of the zeolite structure. The radiation damage, especially amorphization, can significantly reduce the ion exchange capacity for Cs. The breakage of Al–O bonds, the direct displacement of Na^+ to non-exchangeable sites, and the collapse of channel apertures may all account for the decrease in the ion exchange capacity.

Acknowledgements

The H^+ irradiation was conducted at the Michigan Ion Beam Laboratory at the University of Michigan. The SEM, TEM and EMPA were conducted at the Electron Microbeam Analysis Laboratory at the University of Michigan. This work is supported by the Department of Energy's Environmental Management Science Program through grant DE-FG07-97ER45652.

References

1 H. S. Sherry, *Adv. Chem. Ser.*, 1971, **101**, 350.
2 D. C. Grant, A. K. Saha, D. K. Poletz and M. C. Skiba, *AIChE Symp. Ser.*, 1998, **84**, 26413.
3 J. K. Reilly, P. J. Grant, G. J. Quinn, T. C. Runion and K. J. Hofstetter, *ASTM Spec. Tech. Publ.*, 1985, **2**, 1238.
4 National Research Council, *A Study of the Isolation System for Geologic Disposal of Radioactive Waste*, National Academy Press, Washington, DC, 1983.
5 P. K. Sinha and V. Krishnasamy, *J. Nucl. Sci. Technol.*, 1996, **33**, 333.
6 H. Mimura and T. Kanno, *J. Nucl. Sci. Technol.*, 1985, **22**, 284.
7 R. C. Ewing, W. J. Weber and J. F. W. Clinard, *Prog. Nucl. Energy*, 1995, **2**, 63.
8 W. L. Gong, L. M. Wang, R. C. Ewing, E. Vernaz, J. K. Bates and W. L. Ebert, *J. Nucl. Mater.*, 1998, **254**, 249.
9 A. Fortner and J. K. Bates, *Mater. Res. Soc. Symp. Proc.*, 1996, **412**, 205.
10 S. X. Wang, L. M. Wang and R. C. Ewing, *J. Nucl. Mater.*, 2000, **278**, 233.
11 B. X. Gu, L. M. Wang and R. C. Ewing, *J. Nucl. Mater.*, 2000, **278**, 64.
12 B. G. Storey and T. R. Allen, *Mater. Res. Soc. Symp.*, 1998, **481**, 413.
13 L. M. Wang, S. X. Wang and R. C. Ewing, *Proceedings of the International High-Level Radioactive Waste Management Conference*, American Nuclear Society, La Grange Park, Illinois, 1998, p. 772
14 L. V. C. Rees and C. J. Williams, *Trans. Faraday Soc.*, 1965, **61**, 1481.
15 G. V. Tsitsishvili, T. G. Andronikashvili, G. N. Kirov and L. D. Filizova, *Nature Zeolite*, Ellis Horwood, New York, 1992.
16 B. M. Barrer, J. A. Davis and L. V. C. Rees, *J. Inorg. Nucl. Chem.*, 1968, **30**, 3333.

17 P. P. Lai and L. V. C. Rees, *J. Chem. Soc., Faraday Trans. 1*, 1976, **72**, 1809.
18 S. H. Sherry, *J. Phys. Chem.*, 1966, **70**, 1158.
19 P. Sylvester and A. Clearfield, *Solvent Extr. Ion Exch.*, 1998, **16**, 61527.
20 S. M. DePaoli and J. J. Perona, *AIChE J.*, 1996, **42**, 3434.
21 G. L. Palau and K. K. S. Pillay, *Trans. Am. Nucl. Soc.*, 1982, **43**, 113.
22 K. K. S. Pillay, *J. Radioanal. Nucl. Chem.*, 1986, **102**, 247.
23 E. A. Daniels and M. Puri, *Radiat. Phys. Chem.*, 1986, **27**, 225.
24 E. A. Daniels and M. Puri, *Radiat. Eff.*, 1985, **90**, 205.
25 E. A. Daniels and M. Puri, *Int. J. Appl. Radiat. Isot.*, 1985, **36**, 291.
26 G. F. Bastin, F. J. J. van Voo and H. J. M. Heijligers, *X-Ray Spectrom.*, 1984, **13**, 91.
27 J. F. Ziegler, http://www.research.ibm.com/ionbeams/SRIM.
28 M. M. J. Treacy and J. M. Newsam, *Ultramicroscopy*, 1987, **23**, 411.
29 D. R. Acosta, G. Vazquez-polo, R. Garcia and V. M. Castano, *Radiat. Eff. Defects Solids*, 1993, **127**, 37.
30 J. S. Williams and J. M. Poate, *Ion Implantation and Beam Processing*, Academic Press, New York, London, 1984.
31 D. W. Breck, *Zeolite Molecular Sieves–Structure, Chemistry and Use*, Krieger Publishing Company, Malabar, Florida, 1984.
32 L. A. Bursill, E. A. Lodge and J. M. Thomas, *Nature*, 1980, **286**, 111.
33 R. Rudham and A. Stockwell, *Catalysis*, Specialist Periodical Reports, vol. 1, The Chemical Society, London, 1977, p. 87
34 R. Csencsits and R. Gronsky, *Ultramicroscopy*, 1987, **23**, 421.
35 P. Norby, F. I. Poshni, A. F. Gualtieri, J. C. Hanson and C. P. Grey, *J. Phys. Chem. B*, 1998, **102**, 839.
36 A. Maubert, *Zeolite*, 1993, **13**, 587.
37 Y. Sasaki, T. Suzuki and Y. Ikuhara, *J. Am. Ceram. Soc.*, 1995, **78**, 1411.
38 L. A. Bursill, J. M. Thomas and K. J. Rao, *Nature*, 1981, **289**, 157.
39 B. A. Pluijm, J. H. Lee and D. R. Peacor, *Clays Clay Miner.*, 1988, **36**, 498.
40 P. P. Lai and L. V. C Rees, *J. Chem. Soc., Faraday Trans. 1*, 1976, **72**, 1818.
41 P. P. Lai and L. V. C. Rees, *J. Chem. Soc., Faraday Trans. 1*, 1976, **72**, 1827.
42 Y. Yokota, H. Hashimoto and T. Yamaguchi, *Ultramicroscopy*, 1994, **54**, 207.